



January 2020

Investigation Of Aerosol Induced Cold Bias In Numerical Weather Prediction Model Forecasts In Selected Regions On A Global Scale

Xiao Ma

Follow this and additional works at: <https://commons.und.edu/theses>

Recommended Citation

Ma, Xiao, "Investigation Of Aerosol Induced Cold Bias In Numerical Weather Prediction Model Forecasts In Selected Regions On A Global Scale" (2020). *Theses and Dissertations*. 3109.
<https://commons.und.edu/theses/3109>

This Thesis is brought to you for free and open access by the Theses, Dissertations, and Senior Projects at UND Scholarly Commons. It has been accepted for inclusion in Theses and Dissertations by an authorized administrator of UND Scholarly Commons. For more information, please contact und.common@library.und.edu.

Investigation of Aerosol Induced Cold Bias in Numerical Weather Prediction Model
Forecasts in Selected Regions on a Global Scale

by

Xiao Ma
Bachelor of Science, University of Nanjing University of Information and Technology,
2011

A Thesis
Submitted to the Graduate Faculty

of the

University of North Dakota

In partial fulfillment of the requirements

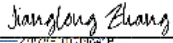
for the degree of

Master of Science

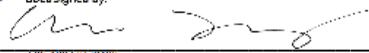
Grand Forks, North Dakota

May
2020


This thesis _____, submitted by Xiao Ma _____ in partial fulfillment of the requirements for the Degree of Master of Science in Atmospheric Sciences from the University of North Dakota, has been read by the Faculty Advisory Committee under whom the work has been done and is hereby approved.

DocuSigned by:


Jianglong Zhang

DocuSigned by:


Aaron Kennedy

DocuSigned by:


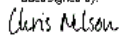
Baike Xi

Name of Committee Member 3

Name of Committee Member 4

Name of Committee Member 5

This thesis _____ is being submitted by the appointed advisory committee as having met all of the requirements of the School of Graduate Studies at the University of North Dakota and is hereby approved.

DocuSigned by:


Chris Nelson
Dean of the School of Graduate Studies

5/6/2020

Date

PERMISSION

Title Investigation of Aerosol Induced Cold Bias in Numerical Weather Prediction
Model Forecasts in Selected Regions on a Global Scale

Department Atmospheric Science

Degree Master of Science

In presenting this thesis in partial fulfillment of the requirements for a graduate degree from the University of North Dakota, I agree that the library of the University shall make it freely available for inspection. I further agree that permission for extensive copying for scholarly purposes may be granted by the professor who supervised my thesis work or, in his absence, by the chairperson of the department or the dean of the Graduate School. It is understood that any copying or publication or other use of the thesis or part thereof for financial gain shall not be allowed without my written permission. It is also understood that due recognition shall be given to me and to the University of North Dakota in any scholarly use which may be made of any material in my thesis.

Xiao Ma

May 5th, 2020

TABLE OF CONTENTS

CHAPTER

I.	INTRODUCTION	1
II.	DATASET	4
	Integrated Surface Database (ISD)	4
	Numerical Forecast Models	6
	The Global Forecast System (GFS) from NCEP	6
	United Kingdom Met Office (UKMO) Forecast Model	7
	MODIS Aerosol Data	7
	Aerosol Robotic Network (AERONET) Observations	8
III.	METHODOLOGY	11
	Data Colocation and Binning Processes	12
	Data Screening for ISD Data	13
	Linear Regression Method	14
	Aerosol Angstrom Exponent	16
	Sky Condition Determination	16
IV.	RESULTS AND DISCUSSION	19
	Inter-comparison with A Previous Study	19
	Seasonal Distributions of AOD and Aerosol Induced Bias in Modeled Near Surface Temperature	20
	The Relation of AOD and ΔT over Clear Free Skies	23
	Impacts of Cloud Contamination on Aerosol Cooling Effects	28
	Impact of Aerosol Type on Aerosol Surface Cooling	30
	Aerosol Cooling Induced Bias as A Function of Forecast Hours	32
	Uncertainties of this study	35
V.	CONCLUSIONS	37
	APPENDIX	39
	REFERENCES	43

LIST OF FIGURES

FIGURE		PAGE
1.	SPATIAL DISTRIBUTION OF ISD STATIONS USED IN THIS STUDY (12406 STATIONS). EACH BLUE SPOT REPRESENTS A GROUND-BASED STATION WITH VALID DATA FOR THE PERIOD OF 2014-2017	5
2.	DIFFERENCES (ΔT) IN TEMPERATURE BETWEEN ISD DATA AND MODELED DATA FROM (A) NCEP AND (B) UKMO UNDER CLOUD-FREE CONDITION OVER NORTHERN HEMISPHERE SPRING FOR THE EAST ASIA REGION. BLUE DOTS REPRESENT ΔT VALUES THAT ARE WITHIN MEAN $\pm 3X$ STANDARD DEVIATION OF ΔT VALUES FOR A GIVEN AOD INTERVAL OF 0.1. RED DOTS REPRESENT ΔT VALUES THAT FAIL THE STANDARD DEVIATION TEST	14
3.	COMPARISON OF THE LINEAR REGRESSIONS OF 51 DATA POINTS BY USING THE LEAST SQUARES METHOD (RED LINE), THEIL-SEN METHOD (GREEN LINE) AND THE ORIGINAL SLOPE EXCLUDING THE OUTLIERS (BLACK LINE)	15
4.	BOX-WHISKER PLOTS OF SEASONAL AVERAGED CLOUD FRACTIONS FROM MODIS FOR THREE ISD REPORTED CLOUD CONDITIONS FOR (A) SPRING, (B) SUMMER, (C) FALL AND (D) WINTER SEASONS USING THREE YEARS OF DATA (2015-2017). RED LINES REPRESENT THE MEDIAN VALUES OF CLOUD FRACTION FOR GIVEN SKY COVERAGE CONDITIONS	18
5.	(A) AQUA MODIS AOD DISTRIBUTION (AT 550NM) OVER ISD STATIONS FOR THE UPPER MID-WESTERN UNITED STATES FOR JUNE 29TH, 2015; (B) SCATTER PLOT OF TEMPERATURE BIASES FROM NCEP MODELED 2-M TEMPERATURE (OBSERVATION TEMPERATURE - FORECASTED TEMPERATURE; IN $^{\circ}C$) AND MODIS AOD USING THE COLLOCATED DATA FROM (A)	20
6.	3-YEAR AVERAGED SEASONAL MEAN AOD (AT 550NM) OVER ISD STATIONS FOR NORTHERN HEMISPHERE (A) SPRING, (B) SUMMER, (C) FALL AND (D) WINTER. RED BOXES HIGHLIGHT FOCUSED STUDY REGIONS	22
7.	3-YEAR AVERAGED SEASONAL MEAN 2-M TEMPERATURE BIASES (OBSERVATION TEMPERATURE - FORECASTED TEMPERATURE IN $^{\circ}C$) FOR NCEP MODEL OVER ISD STATIONS FOR NORTHERN HEMISPHERE (A) SPRING, (B) SUMMER, (C) FALL AND (D) WINTER. RED BOXES HIGHLIGHT FOCUSED STUDY REGIONS	23
8.	3-YEAR AVERAGED SEASONAL MEAN 2-M TEMPERATURE BIASES (OBSERVATION TEMPERATURE - FORECASTED TEMPERATURE, IN $^{\circ}C$) FOR UKMO MODEL OVER ISD STATIONS FOR NORTHERN HEMISPHERE (A) SPRING, (B) SUMMER, (C) FALL AND (D) WINTER. RED BOXES HIGHLIGHT FOCUSED STUDY REGIONS	41

LIST OF TABLES

TABLES	PAGE
1. CLASSIFICATION OF SKY CONDITIONS	6
2. DETAIL INFORMATION OF THE EIGHT FOCUSED REGIONS	11
3. UTC TIME FOR REGIONS THAT EXPERIENCE LOCAL DAYTIME	12
4. SEASONAL VARIATIONS OF SLOPES (WITH 95% CONFIDENCE INTERVALS), TEMPERATURE BIASES AND MEAN AODS OF EIGHT FOCUSED REGIONS UNDER CLOUD-FREE CONDITION USING NCEP DATA	24
5. SIMILAR TO TABLE 4, BUT FOR USING UKMO DATA.....	26
6. AEROSOL COOLING EFFICIENCY ($^{\circ}\text{C}/\text{T } 550\text{nm}$) UNDER THREE SKY CONDITIONS FOR NCEP AND UKMO MODELS FOR SPRING FOR THREE SELECTED REGIONS. ALSO INCLUDED ARE MEAN MODIS AOD, AEROENT ANGSTROM EXPONENT (A) AND 95% CONFIDENT INTERVALS FOR SLOPES (AEROSOL COOLING EFFICIENCIES).....	28
7. SIMILAR TO TABLE 6, BUT FOR THE SUMMER SEASON	29
8. SIMILAR TO TABLE 6, BUT FOR THE FALL SEASON	29
9. SIMILAR TO TABLE 6, BUT FOR THE WINTER SEASON	30
10. SEASONAL VARIATIONS OF AEROSOL COOLING EFFICIENCY ($^{\circ}\text{C}/\text{T } 550\text{nm}$) FOR THE EAST ASIA, INDIA AND THE MIDDLE EAST REGIONS UNDER CLOUD-FREE CONDITION USING NCEP AND UKMO DATA	31
11. THE VARIATIONS OF SEASONAL-BASED AEROSOL COOLING EFFICIENCY ($^{\circ}\text{C}/\text{AOD}$) FOR 0H, 24H AND 48H FORECASTS FOR THE EAST ASIA AND INDIA REGIONS USING NCEP MODEL DATA. ALSO INCLUDED ARE FORECASTING PERIODS, 95% CONFIDENT INTERVALS OF THE COMPUTED SLOPES AS WELL AS MEAN AND MEDIAN OF ΔT VALUES	32
12 SIMILAR TO TABLE 11, BUT FOR USING UKMO MODEL DATA.....	33
13. TOTAL NUMBER OF MISSING DATA FROM NCEP MODEL (DATA ARE NOT AVAILABLE FROM THE TIGGE SITE), ‘-’ REPRESENTS NO MISSING DATA FOR CURRENT FORECAST PERIOD.	40
14.SAME AS TABLE 13, BUT FOR UKMO MODEL	40
15. ACRONYMS AND DEFINITIONS.	42

ACKNOWLEDGEMENTS

I would like to thank my advisor, Dr. Jianglong Zhang for his support and feedback throughout the course of this thesis project. I also thank Dr. Aaron Kennedy and Dr. Baike Xi for their comments and suggestions during the project. I would also like to thank my friends and fellow graduate students who provided relief and helped mold my graduate school experience. Finally, I thank my family for their love and support, and for encouraging me to always pursue my dreams.

ABSTRACT

Using surface observations from the Integrated Surface Database (ISD), remotely sensed data from Moderate Resolution Imaging Spectroradiometer (MODIS), and modeled data from National Centers of Environmental Prediction (NCEP) and United Kingdom Met Office (UKMO) models, the aerosol induced surface cooling effect is studied for eight selected regions. The results of this study indicate that aerosol plumes could impact surface temperature forecasts for all four seasons in East Asia and India and for seasons with heavy aerosol plumes in the Middle East and South Africa. No clear signals are found for either the impact of cloud contamination or the impact of aerosol type on the aerosol cooling effect. Overall, the findings of the study suggest the need for including aerosols in numerical forecasts for regions that experience heavy aerosol plumes, as well as highlights the regions and seasons that would require the consideration of such an effort.

CHAPTER 1

INTRODUCTION

Aerosol particles include sea salt, black carbon, organic carbon, dust and pollutants, with different source and sink mechanisms associated with various aerosol types within distinct regions. These particles, as a common component of the atmosphere, are known to have a non-trivial effect on climate through alteration of the radiation balance of the earth-atmospheric system. Aerosol particles can affect climate directly, through scattering and absorbing short-wave radiation during daytime and absorption, and emission of long-wave radiation for both day- and night-time (Coakley et al., 1992). Indirectly, aerosol particles can act as cloud condensation nuclei (CCN), changing cloud particle size and distribution, further affecting precipitation (Wang et al., 2014). Semi-indirectly, aerosol particles could absorb solar energy, heat the air column and thus alter cloud properties (Painemal and Zuidema, 2013).

Alternatively, aerosol particles could have both direct and indirect effects on weather, as well as introduce perturbations to surface and atmospheric properties such as changes in surface temperature, wind patterns and regional precipitation activities (e.g. Zhang et al., 2016). Observational evidences have been reported for the impacts of dust storms or smoke plumes from wildfires on meteorological properties. For example, Zhang et al. (2016) showed that biomass burning aerosol plumes could introduce a 2-5 °C drop in surface temperature, and an estimated aerosol cooling efficiency of 1.5 °C per unit aerosol optical depth (AOD) at 550 nm, during a biomass burning aerosol episode that occurred in summer 2015 over the Northern Great Plains.

Similarly, modeling based studies have reported the potential changes in various meteorological parameters due to aerosol events. For example, a simulation experiment (Benedetti and Vitart, 2018) showed that the presence of aerosol particles had reduced wind speed and precipitation amounts in East Asia by approximately $1\text{-}2\text{ m s}^{-1}$ and $0.5\text{-}1\text{ mm day}^{-1}$, respectively.

Although recent observational and modeling studies have indicated the impacts of aerosol particles on weather patterns, unlike climate models, aerosol particles are often not considered in numerical weather forecasts. This is partially because the impacts of aerosol particles on weather are not well understood. Also, justification is needed for the inclusion of aerosol particles in numerical weather forecasts due to the additional computational expenses of inclusion of associated processes.

Therefore, it is necessary to study the impacts of aerosol particles on weather forecasts, at both regional and global scales to quantify the necessity of including aerosol particles in numerical weather forecasts. In this thesis, the uncertainties of forecasted near surface temperatures in the United Kingdom Met Office (UKMO) and the National Centers for Environmental Prediction (NCEP) are investigated as functions of aerosol properties. Modeled temperatures are compared to observed temperatures from the integrated surface database (ISD) stations, with aerosol properties over the study scenes quantified using retrievals from the Moderate Resolution Imaging Spectroradiometer (MODIS) and ground-based observations from the Aerosol Robotic Network (AERONET). This study focuses on answering the following questions:

1. Do aerosol cooling effects vary spatially and temporally across multiple scales?

2. While aerosol cooling effects are often quantified over cloud free skies, what are aerosol cooling effects be under partially cloud covered skies?
3. What are the impacts of aerosol particles on short-term weather forecasted temperatures?
4. Do dust and smoke aerosol particles have different aerosol cooling effects?

The thesis is divided into the following sections: Chapter 2 introduces the data sources, Chapter 3 includes the methodology of the study, Chapter 4 discusses the results from the analysis, and Chapter 5 summarizes the discussions and future outlook of this research.

CHAPTER 2

DATASET

This section describes the data used in this study. These datasets include 2-m temperature analyses and forecasts from the Global Forecast System (GFS) from NCEP and the Unified model from UKMO; observed surface temperatures and sky conditions from the Integrated Surface Database (ISD) and AOD data from Aerosol Robotic Network (AERONET) and Moderate Resolution Imaging Spectroradiometer (MODIS) collection 6.1 Dark Target (DT) aerosol products.

2.1 Integrated Surface Database (ISD)

ISD data include meteorological parameters such as temperature, dewpoint, wind speed and direction, precipitation, cloud fraction, and snow depth (Lott et al., 2001) with unified parameter units under the same time scale compare to modeled forecast period (in UTC). Quality control steps are applied which include cross checks among related stations and the implementation of an automated correction system (<https://www.ncdc.noaa.gov/isd>).

In this study, the surface temperature (in °C) and sky condition (in 0-6 oktas) were used to evaluate modeled temperature values under different sky conditions (source: <ftp://ftp.ncdc.noaa.gov/pub/data/noaa/isd-lite>). Figure 1 shows the map of the stations used in the study, which represents a total of 12,406 stations for the period of year 2014-2017.

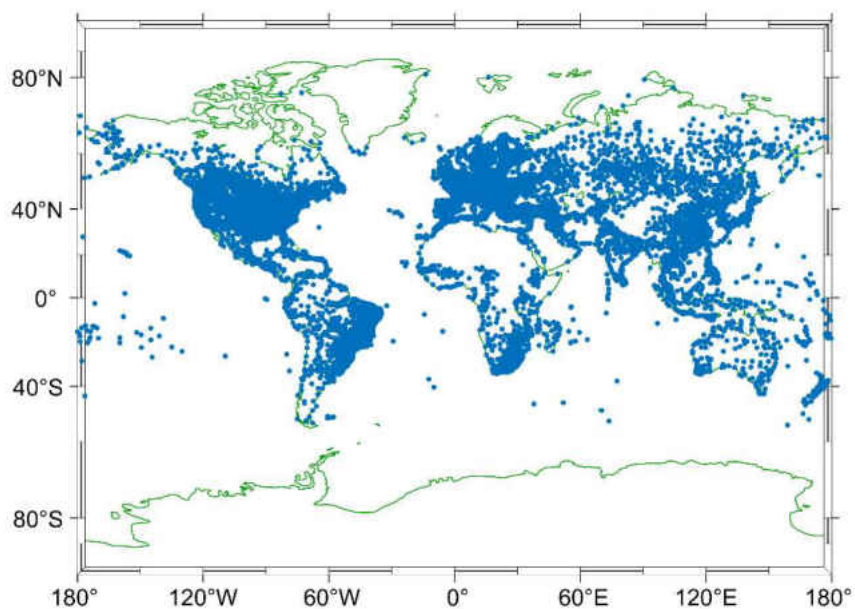


Figure 1. Spatial distribution of ISD stations used in this study (12406 stations). Each blue spot represents a ground-based station with valid data for the period of 2014-2017.

The sky condition is classified based on cloud or other obscuring phenomena (source: <ftp://ftp.ncdc.noaa.gov/pub/data/noaa/isd-format-document.pdf>). The unit scale of sky condition is given by Table 1.

Table 1. Classification of sky conditions

(source: <ftp://ftp.ncdc.noaa.gov/pub/data/noaa/isd-lite/isd-lite-format.txt>)

Cloud cover units	Sky cover condition
0: None	SKC or CLR
1: One okta	1/10 or less but not zero
2: Two oktas	2/10 – 3/10, or FEW
3: Three oktas	4/10
4: Four oktas	5/10, or SCT
5: Five oktas	6/10
6: Six oktas	7/10 – 8/10
7: Seven oktas	9/10 or more but not 10/10, or BKN
8: Eight oktas	10/10, or OVC

2.2 Numerical Forecast Models

Data from two different numerical weather forecasting models, UKMO and NCEP, were obtained from the THORPEX Interactive Grand Global Ensemble (TIGGE) data archive (source: <https://apps.ecmwf.int/datasets/data/tigge/levtype=sfc/type=cf/>). In this study, 2-m surface temperature data from NCEP and UKMO models with the same forecast periods and time step were used.

2.2.1 The Global Forecast System (GFS) from NCEP

The GFS is a weather forecast model from NCEP (source: <https://www.ncdc.noaa.gov/data-access/model-data/model-datasets/global-forecast->

system-gfs). The model provides analyses and forecasts on a wide range of weather parameters that include surface temperature, winds, precipitation, soil moisture and atmospheric ozone concentration. The Grid Point Statistical Interpolation (GSI) is used as the data assimilation scheme (Kleist et al. 2009) for improving accuracies of initial conditions. The NCEP data used in this study include global forecasts of meteorological parameters four times a day at 0000, 0600, 1200 and 1800 UTC on a $0.5^\circ \times 0.5^\circ$ grid with a 3-hour time step and up to a +384 hours forecast period.

2.2.2 United Kingdom Met Office (UKMO) Forecast Model

The UKMO model is a unified global numerical weather prediction model. Similar to NCEP GFS, a 4-D Var data assimilation method (Hamill T., 2011) has been incorporated for generating mean initial conditions. The UKMO model reports meteorological parameters four times a day at the same UTC times as compared to the GFS with up to a +174 hours forecast period. The UKMO data used in this study including forecasted temperature of 0h, 24h and 48h at a spatial resolution of $0.5^\circ \times 0.5^\circ$ grid with a 3-hour time step.

Note that missing data exist for both NCEP and UKMO data for the selected study period; a compiled list of those missing data is included in Appendix A.

2.3 MODIS Aerosol Data

The collection 6.1 Level-2 DT Aqua MODIS AOD data (approximately 1:30 local overpass time) were used in this study. The MODIS DT algorithm, which applied on both over land and ocean retrievals, is based on the assumption that aerosols brighten dark surface regions. The retrieval process is performed by matching observed radiance values

with top of atmosphere (TOA) radiance values from a pre-computed look up table (LUT) (Levy et al., 2010). For the land retrieval, the brightest 50% and the darkest 20% of pixels are removed for screening out unwanted features such as clouds, water, and snow/ ice pixels. The expected errors for current DT AOD retrievals at 10-km resolution are $[\pm (0.05 + 15\%)]$ and $[\pm (0.03 + 5\%)]$, for ocean land and over ocean AOD retrievals respectively (e.g. Levy et al., 2013).

The spatial resolution of the MODIS DT aerosol products is 10 km with the DT aerosol optical depth retrievals available at 7 wavelengths (centered on 470nm, 550nm, 650nm, 860nm, 1240nm, 1640nm, and 2110 nm) over ocean and 3 wavelengths (centered on 470nm, 650nm, and 2110nm) over land. For this study only DT Aqua AOD values at the 550nm are used. Pixels are further quality controlled such that only the “best” quality over land (QA = 3) and “marginal” to “best” quality over ocean retrievals (QA = 1, 2, or 3) were utilized in this study.

Cloud mask data are also included in the MODIS aerosol products. The cloud mask data were further used to inter-compare with cloud fractions as reported from the ISD data in this study.

2.4 Aerosol Robotic Network (AERONET) Observations

AERONET data are a global collection of ground observations of aerosol properties from approximately 400 sun-photometer stations, with data from 311 stations used in this study. The sun-photometer instruments measure sun and sky radiances at 7 spectral bands ranging from 340 nm to 1640 nm which are further used for retrieving of aerosol optical and physical properties (Holben et al., 1998). Aerosol optical depths, which are the primary

product of sun-photometer measurements, are computed through Beer-Bouguer's Law by accounting for attenuation of solar energy by aerosols. For sky measurements, two sky observation sequences, 'almucantar' and 'principal plane' are performed at 440nm, 670 nm, 870 nm and 1020 nm (Holben et al., 1998) for retrieving related aerosol properties such as aerosol absorption and size parameters. In this study, only quality controlled and cloud screened version 3, level 2 AERONET data were used. The reported uncertainty for AERONET AOD is on the order of ± 0.01 per optical air mass (Giles et al., 2019).

Note, no measurements at 550 nm is available from the sun-photometer instruments; yet, to be consistent with MODIS AOD retrievals, AERONET AOD values are interpolated to 550 nm using 440 nm and 675 nm AERONET data based on the equation as shown below, which assumes a constant Angstrom exponent value between 440nm-550nm and 550nm to 670 nm,

$$\frac{\tau_{\lambda}}{\tau_{\lambda_0}} = \left(\frac{\lambda}{\lambda_0}\right)^{-\alpha} \quad (1)$$

where τ_{λ_0} and τ_{λ} are the AOD values at reference wavelengths of λ_0 and λ respectively. The Angstrom exponent parameter α is defined by equation 2 based on the log of ratio of τ_{λ} and τ_{λ_0} and the log ratio of λ and λ_0 .

$$\alpha = -\frac{\lg\frac{\tau_{\lambda}}{\tau_{\lambda_0}}}{\lg\frac{\lambda}{\lambda_0}} \quad (2)$$

In addition, fine model aerosol fraction data from AERONET are also used to assist in discriminating aerosol types in this study. The fine model aerosol fraction refers as the ratio of fine mode aerosol optical depth to total aerosol optical depth, estimated based on the spectral de-convolution algorithm (SDA) as illustrated in O'Neill et al. (2003). Fine

mode fraction values range from 0 to 1 with 0 means all coarse model aerosols (particle size typically larger than 1 μm) and 1 means all fine model aerosols (particle size typically around or less than 0.25 μm). Fine mode fraction data are included in the AERONET data used in this study.

CHAPTER 3

METHODOLOGY

In this chapter, data processing and analysis methods are discussed. Note that different type of aerosol plumes could exist at different regions and for different seasons. For example, dust aerosol is the dominant aerosol type over East Asia during the spring season, while pollutant aerosols are the primary aerosol during the winter seasons for East Asia (Zhang et al., 2017). Thus, regional-based analyses were implemented for eight selected regions, which have heavy aerosol plumes (e.g. have days with AOD at 550nm > 0.3) for one or more seasons. The selected regions, as well as the latitude and longitude boundaries of the selected regions are listed in Table 2.

Table 2. Detail information of the eight focused regions.

Area	Location (Lon/Lat)
East Asia	9.71 N-40.98N; 95.68E-126.63E
Europe	36.00N-71.13N; 9.52W-66.17E
India	8.00N-36.00N; 68.00E-97.00E
North-east Asia	45.91N-60.94N; 102.37E-144.64E
US	25.00N-49.00N; 73.00W-125.00W
The Middle East	12.27N-36.59N; 37.83E-61.80E
Mid-south Africa	17.11S-2.41N; 7.41E-44.75E
South America	18.86S-2.49W; 45.36W-82.30W;

3.1 Data Colocation and Binning Processes

To study the temporal variations of aerosol cooling effects, a total of three years (December 2014 to November 2017) of ground based and satellite observations, as well as analyses and forecasts from NCEP and UKMO models were processed for four Northern Hemisphere seasons: spring (March, April, May), summer (June, July, August), fall (September, October, November), and winter (December (from previous year), January, February). In addition, analyses and forecasts of UKMO and NCEP are only available at four discrete times: 00:00, 06:00, 12:00 and 18:00 UTC. To account for the time discrepancy between modeled data and the ISD, AERONET and MODIS data, the observational data are rebinned into those four time windows. For example, observational data from 03:00-09:00UTC are grouped for inter-comparing with model data at 06:00UTC. Also, since AERONET and MODIS data are only available at daytime, for a given region, only daytime ISD and model (UKMO and NCEP) data are used as shown in Table 3 with nighttime ISD and model data discarded.

Table 3. UTC Time for regions that experience local daytime.

Longitude (degree)	Time zone
45E~135E	06:00UTC
45W~45E	12:00UTC
135W~45W	18:00UTC
180W~135W, 135E~180E	00:00UTC

3.2 Data Screening for ISD Data

Despite existing quality control steps for ISD data, erroneous ISD data are still observable, represented by abnormally low and high temperatures found in the dataset. To exclude those noisy ISD data, a three-standard deviation data screening step is applied where the differences between ISD and modeled temperatures (ΔT) are evaluated against MODIS AOD. The MODIS AOD data are divided into 0.1 AOD bins in which mean and standard deviation of (ΔT) are computed. ISD temperature data that have ΔT values outside the mean $\pm 3 \times$ standard deviation are assumed to be erroneous data and are excluded in the analysis.

An example of this method is shown in Figure 2 where panels (a) and (b) shows the scatter plot of collocated ΔT and AOD for the East Asia region for Northern Hemisphere Spring, using NCEP and UKMO analyses data (0h forecast time), respectively. ΔT is computed using the difference between collocated ISD and the model temperature data. The red points are raw data and blue points are data pairs that passed the 3-standand deviation data screen method.

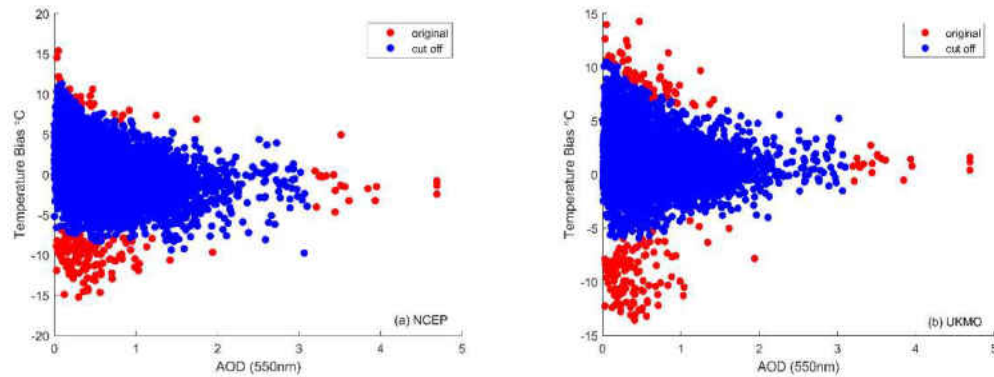


Figure 2. Differences (ΔT) in temperature between ISD data and modeled data from (a) NCEP and (b) UKMO under cloud-free condition during Northern Hemisphere Spring for the East Asia region. Blue dots represent ΔT values that are within mean $\pm 3 \times$ standard deviation of ΔT values for a given AOD interval of 0.1. Red dots represent ΔT values that fail the standard deviation test.

3.3 Linear Regression Method

The regression between ΔT and MODIS AOD is studied using the Theil-Sen linear regression method. The Theil-Sen linear regression method was first proposed by Theil. (1950) as a median slope estimator and expanded later by Sen. (1968) into handle pairwise slopes. Compared to the least square method, the Theil-Sen regression method is less sensitive to outliers and can tolerate arbitrary corruption of up to 29.3% of outliers without decreasing the accuracy (Rousseeuw et al., 2003). In this study, this regression method is used to calculate the slope and intercept of the relationship between surface temperature bias and AOD values for study areas.

As an example, Figure 3 shows the comparison between the Theil-Sen estimator and the least square estimator. A total of 51 sample data points were generated that have a slope of two. A total of 20% outliers are also included. The linear regression results of slopes calculated by both Theil-Sen estimator and least square are 1.87 and 1.29, respectively. As shown in Figure 3, the linear regression from Theil-Sen estimator has a

closer convergence with the original slope which indicates that this estimator has better overall performance with datasets that have a high ratio of outliers. We therefore use the method in the remainder of this study in order to minimize the impact of such outliers.

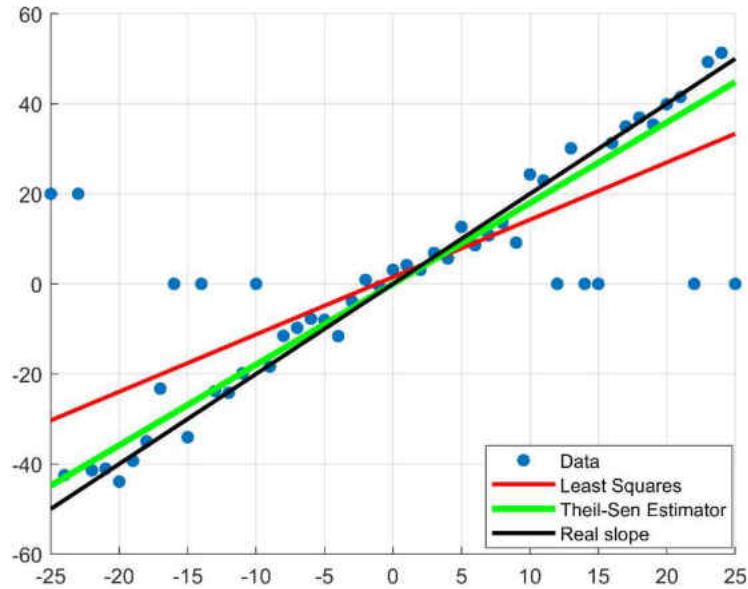


Figure 3. Comparison of the linear regressions of 51 data points by using the least squares method (red line), Theil-Sen method (green line) and the original slope excluding the outliers (black line). Note this is a replicate of an example from <https://www.mathworks.com/matlabcentral/fileexchange/34308-theil-sen-estimator>.

In addition, the confidence intervals for the derived slopes are also computed at a significance level $\alpha=0.05$. For N values of Theil-Sen slopes Q_N , where N value is defined as $N=\frac{n(n-1)}{2}$ and n is the total number of data points, the Q_{med} (or the slope reported by the Theil-Sen method) is the median value computed by ranking Q_N values from the smallest to largest. The confidence interval can be calculated as follows (Gilbert, 1987).

$$C_\alpha = Z_{1-\alpha/2} \sqrt{\text{Var}(S)} \quad (3)$$

Where $Z_{1-\alpha/2}$ is equal to 1.960 for significance level $\alpha=0.05$ (Gilbert, 1987) and $\text{Var}(S)$ is the variance of the Mann-Kendall test statistic S (Mann, 1945; Knedall,1975), which can be calculated through the following equation,

$$\text{Var}(S) = \frac{n(n-1)(2n+5) - \sum_{i=1}^m t_i(t_i-1)(2t_i+5)}{18} \quad (4)$$

Where n is the total number of data points, t_i is the i_{th} tied value, and m is the number of groups with values that are equal or tied (Mann, 1945; Knedall,1975).

Once the value of C_α is calculated, the slope values of $M_1 = \frac{N - C_\alpha}{2}$ and $M_2 = \frac{N + C_\alpha}{2}$ can be also calculated. Finally, the computed slopes from the Sen's estimator are sorted and the M_1 th and (M_2+1) th largest slopes are used to define the lower and upper limited of the 95% confidence interval (Gilbert, 1987).

3.4 Aerosol Angstrom Exponent

One of the principle questions raised in this study is the examination of aerosol cooling effect as a function of aerosol type. Aerosol type is estimated using the Angstrom exponent (Angstrom,1929), which is a quantitative measure of aerosol particle size. The value of the Angstrom exponent (α) between the 440-675 nm wavelengths is computed using equation (2) from chapter 2. An analysis of Aerosol particle size distribution (Eck et al., 1999) showed that for the α value computed from 440-670 nm wavelengths, a larger value ($\alpha \geq 1$) usually refers urban pollution or biomass burning aerosol particles whereas a smaller value ($\alpha \leq 1$) usually indicates dust or sea salt aerosols.

3.5 Sky Condition Determination

Another component of the study is to evaluate the aerosol cooling effect under different cloud coverage conditions. To achieve this goal, observation scenes are divided into three categories: totally clear, partly cloud cover and most cloud cover conditions.

These are defined as follows: 0 okta represents clear conditions, 1-3 oktas refer partly cloudy condition and finally 4-6 oktas indicate mostly cloudy condition. Near overcast and overcast conditions (7-8 oktas) are not included in this study. Again, table 1 shows the classification of sky conditions used in this study.

The comparison between ISD cloud coverage and MODIS cloud fraction was also made on a seasonal basis using three years (2015-2017) of collocated ISD and MODIS data as shown in Figure 4. To collocate the two datasets, MODIS cloud fraction data that are within $0.3 \times 0.3^\circ$ (Latitude/Longitude) of an ISD ground station are averaged and used to represent cloud fraction for the given station. As indicated from Figure 4, Cloud free scenes as reported from the ISD data (0 okta) represents mean MODIS cloud fraction of less than 20%. The ISD data reported partly cloudy conditions (1-3 oktas) correspond to mean MODIS cloud fraction of around 40% and the ISD data reported mostly cloudy conditions (4-6 oktas) correspond to mean MODIS cloud fraction of around 60-70%. Note that since MODIS data within a $0.3 \times 0.3^\circ$ (Latitude/Longitude) area are used for representing cloud conditions as reported from the ISD data, which may or may not be the precise observational domain as reported by the ISD data. Still, Figure 4 suggests that cloud conditions from the ISD data can be used to represent cloud conditions of the observing scenes.

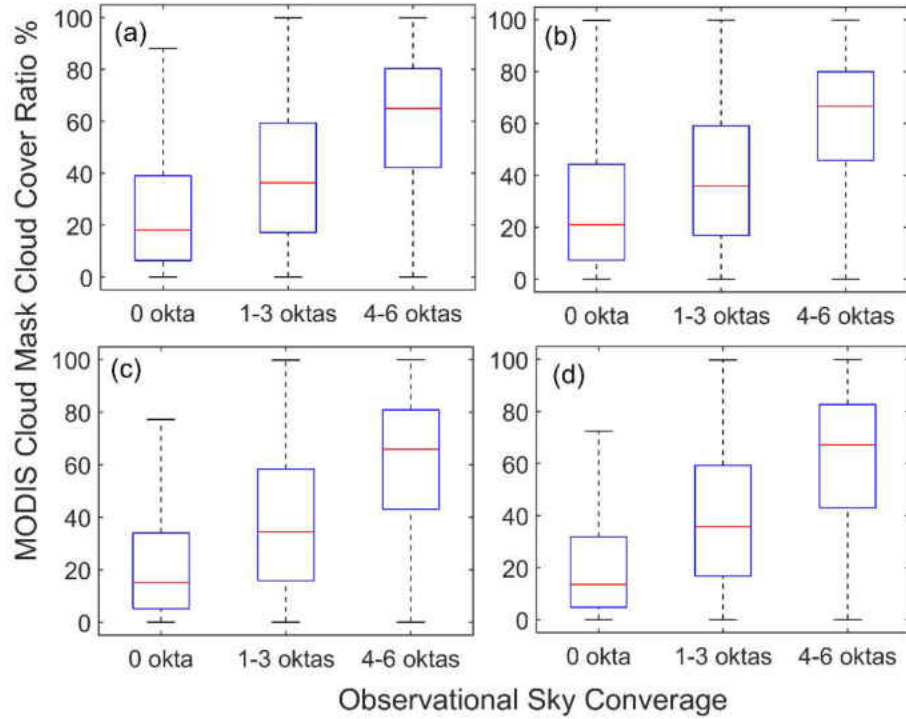


Figure 4. Box-whisker plots of seasonal averaged cloud fractions from MODIS for three ISD reported cloud conditions for (a) spring, (b) summer, (c) fall and (d) winter seasons using three years of data (2015-2017). Red lines represent the median values of cloud fraction for given sky coverage conditions.

CHAPTER 4

RESULTS and DISCUSSION

4.1 Inter-comparison with A Previous Study

In a previous study, Zhang et al. (2016) investigated the smoke surface cooling effect for a significant smoke aerosol episode that occurred in Midwestern United States from June 28th to June 30th, 2015. In Zhang et al. (2016), a daytime direct surface cooling effect around -1.5°C per unit AOD at 550nm wavelength was found over Grand Forks, ND for June 29th, 2015. As a self-evaluation of the algorithms and datasets used in this study, this effort was repeated using collocated data from ground observation stations and NCEP model as well as collocated AOD values at 550nm from MODIS AQUA, as shown in Figure 5. In Figure 5a, each point indicates a collocated pair of MODIS AOD versus the difference between observed near surface temperature and NCEP reported surface temperature (ΔT). To match the reference study as shown in Zhang et al. (2016), the latitude and longitude ranges of the study area are restricted to 40.63° N to 49.63° N and 90.98° E to 104.98° E respectively and as well as the time frame of June 28th to 30th, 2015. As suggested from Figure 5b, while data are rather scattered for the AOD range of 0-0.5, a noticeable near linear pattern is found between MODIS AOD and ΔT for the AOD range of 0.5-5. The slope of AOD versus ΔT is estimated to be -1.55°C per unit AOD at 550nm, which is very similar to the reported aerosol cooling efficiency value as reported by Zhang et al. (2016) of -1.5°C per AOD at 550nm.

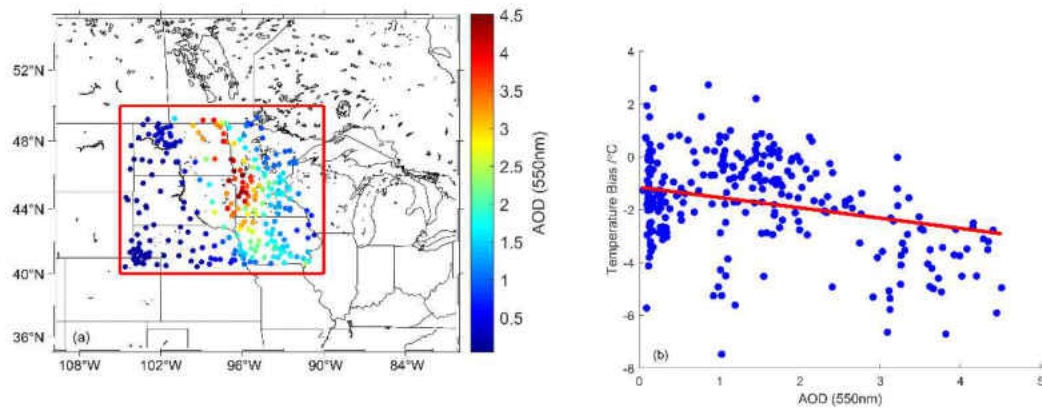


Figure 5. (a) Aqua MODIS AOD distribution (at 550nm) over ISD stations for the upper Mid-western United States for June 29th, 2015; (b) Scatter plot of temperature biases from NCEP modeled 2-m temperature (observation temperature – forecasted temperature; in °C) and MODIS AOD using the collocated data from (a).

4.2 Seasonal Distributions of AOD and Aerosol Induced Bias in Modeled Near Surface Temperature

Encouraged by the consistency between the two case studies, the same method was then applied to a regional analysis for eight selected regions as mentioned in the previous chapter. Using three years (2015-2017) of the collocated dataset, the seasonal-based spatial distribution of Aqua MODIS AODs were studied and are shown in Figure 6 for all ground stations as used in this study; where each point in Figure 6 represents seasonal mean AOD value of a matched station. Note the total amount of data points from each season may vary due to more or less available data from MODIS during certain seasons.

Overall, among four seasons, regions with large AOD value ($AOD > 0.3$) include China and east Asia, India, The Middle East, and Mid-south Africa. For South America and North East Asia, high AOD value are prevalent only during certain seasons; for South America, the peak AOD value is reached during the fall and moderate AOD exists throughout the summer to winter periods. Similarly, for northeast Asia, the high AOD values only persist during summer period. In the remaining regions, US and Europe, there is a consistent pattern of mean AOD value of less than 0.3 for all four seasons.

Similarly, using three years (2015-2017) of collocated dataset, the seasonal-based spatial distribution of the 2-m temperature biases (ΔT ; ground station – NCEP temperature) from NCEP model are shown in Figure 7 (note the same analysis was also conducted using UKMO data, the plots of which are shown in the Appendix B). For both NCEP and UKMO models, the ΔT values have shown strong spatial and temporal variations among study regions. In particular, India has shown negative ΔT patterns throughout the four seasons. Such negative ΔT patterns are not found for other regions. It is unsure if the negative ΔT patterns over India as seen in Figure 7 are due to model inherited uncertainties or due to aerosol cooling effects, as this region is often covered with thick aerosol plumes.

Through a surface-level cross checking between Figures 6 and 7, the relationship between AOD and ΔT seems less observable. This is likely caused by other factors such as uncertainties in the model and observations of surface temperature, as well as potential cloud contamination in space-borne and surface observations, all of which could impact the overall accuracy of the results.

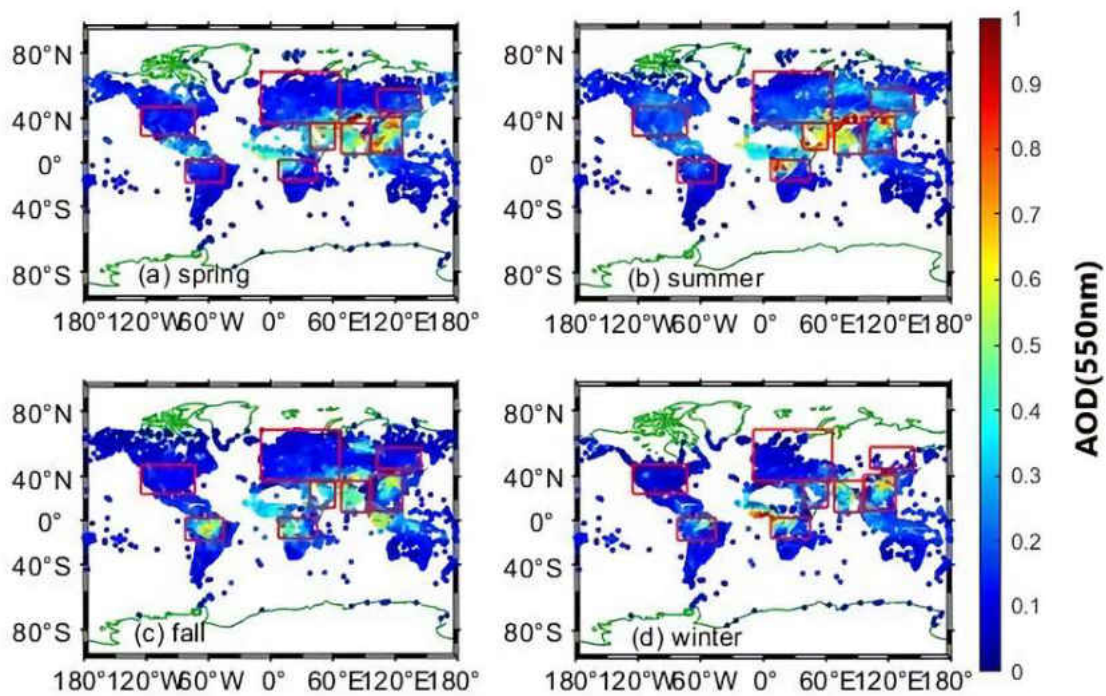


Figure 6. 3-year averaged seasonal mean AOD (550nm) over ISD stations for Northern Hemisphere (a) spring, (b) summer, (c) fall and (d) winter. Red boxes highlight focused study regions.

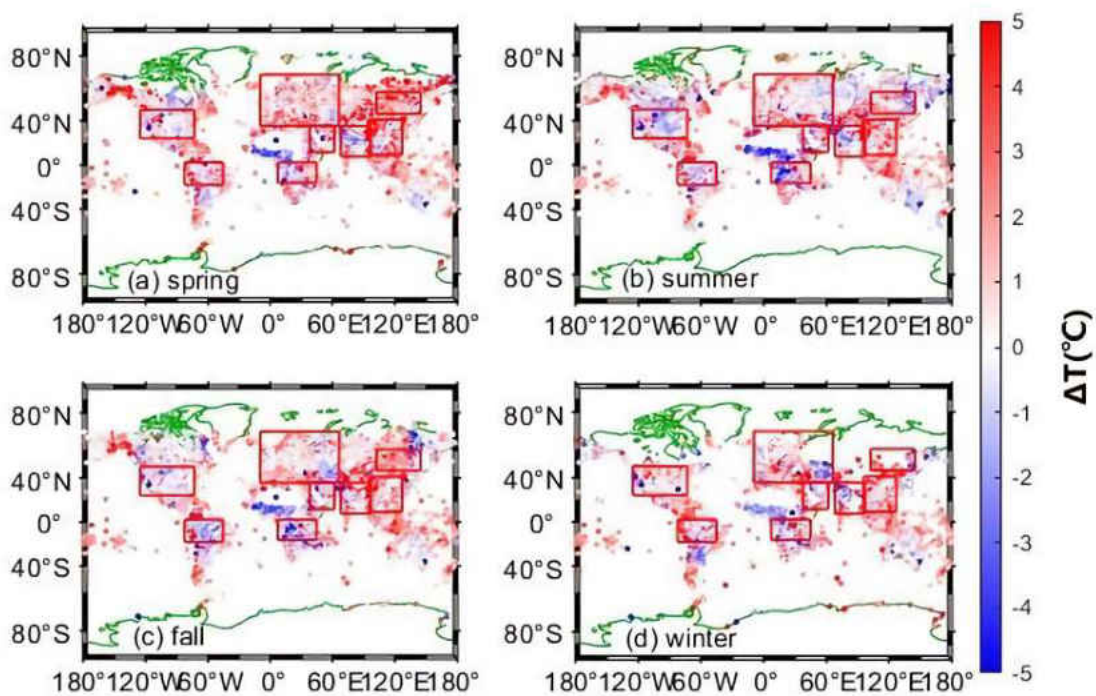


Figure 7. 3-year averaged seasonal mean 2-m temperature biases (observation temperature – forecasted temperature in °C) for NCEP model over ISD stations for Northern Hemisphere (a) spring, (b) summer, (c) fall and (d) winter. Red boxes highlight focused study regions.

Although some regions show relationship between AOD and ΔT for some seasons, especially for regions with high mean AOD value ($AOD > 0.3$), such a relationship is less clear for other regions or seasons. To further explain this phenomena, other factors that might have an impact on the AOD and ΔT relationship, such as cloud contamination and aerosol speciation need to be considered (Painemal and Zuidema, 2013).

4.3 The Relation of AOD and ΔT over Clear Free Skies

As the base study, the relationship of AOD and ΔT (from NCEP) was calculated, as shown in Table 4 for the selected regions using collocated data from cloud free skies, as indicated from the ISD data. Also included in Table 4 are the 95% confident intervals of the reported slopes.

Table 4. Seasonal variations of slopes (with 95% confidence intervals), temperature biases and mean AODs of eight focused regions under cloud-free condition using NCEP data.

Area	Season	Slope	95% confidence interval	Total data points	Mean AOD	AOD value ratio (%)	
						>0.5	>1.0
East Asia	Spring	-2.5	[-2.61, -2.40]	11,182	0.61	46.97	18.13
	Summer	-1.67	[-1.91, -1.42]	2,796	0.46	34.05	10.66
	Fall	-2.23	[-2.39, -2.08]	8,209	0.31	18.61	3.81
	Winter	-0.5	[-0.62, -0.38]	12,698	0.33	20.54	3.84
India	Spring	-2.28	[-2.41, -2.15]	12,553	0.5	41.79	6.87
	Summer	-2.5	[-2.70, -2.30]	3,058	0.96	80.61	43.39
	Fall	-2.75	[-2.87, -2.64]	13,494	0.54	44.03	10.76
	Winter	-2.04	[-2.12, -1.96]	20,323	0.52	39.37	13.22
Europe	Spring	0.03	[0.03,0.03]	27,309	0.14	2.19	0.09
	Summer	0.05	[-0.10, 0.23]	48,714	0.19	3.81	0.24
	Fall	0.06	[-0.24, 0.94]	35,662	0.13	1.88	0.22
	Winter	0.52	[0.52, 0.52]	14,311	0.09	0.49	0
US	Spring	1.89	[1.79, 1.97]	90,068	0.11	0.45	0
	Summer	-1.02	[-1.03, -0.92,]	118,648	0.19	4.95	1.80
	Fall	-0.69	[-1.17, -0.32]	118,753	0.1	2.17	0.76
	Winter	2.11	[1.63, 2.61]	53,245	0.06	0	0
North East Asia	Spring	-3.95	[-5.81, -2.14]	699	0.12	0	0
	Summer	-0.66	[-1.16, -0.15]	1,598	0.24	13.20	4.07
	Fall	-3.47	[-4.51, -2.49]	1,701	0.1	1.88	0
	Winter	-18.17	[-25.69, 15.07]	124	0.11	0	0
	Spring	-4.88	[-9.61, -0.80]	125	0.11	0	0
	Summer	-3.39	[-4.10, -2.70]	1,103	0.23	10.79	0

Area	Season	Slope	95% confidence interval	Total data points	Mean AOD	AOD value ratio (%)	
						>0.5	>1.0
Mid-south Africa	Fall	-0.47	[-1.39, 0.44]	513	0.34	21.44	0
	Winter	-2.63	[-5.82, 0.21]	105	0.53	48.57	0
Middle East	Spring	-0.39	[-0.67, -0.11]	4,360	0.43	29.95	4.50
	Summer	-0.83	[-1.02, -0.64]	6,692	0.51	41.26	6.44
	Fall	-0.56	[-0.80, -0.33]	5,598	0.38	21.04	3.61
	Winter	-1.32	[-1.82, -0.82]	4,316	0.24	5.40	0.25
South America	Spring	2.3	[0.26, 4.35]	847	0.15	0	0
	Summer	0.1	[-1.41, 1.65]	1,986	0.11	0.60	0
	Fall	-3.04	[-3.76, -2.33]	1,399	0.28	13.08	2.57
	Winter	0.12	[-1.80, 2.11]	397	0.22	5.54	0

As shown in Table 4, statistically significant relationships are found between ΔT and AOD for regions and seasons that have mean AOD value over 0.3 in most cases. For those regions, the aerosol cooling effect, which is defined as the aerosol induced surface cooling in $^{\circ}\text{C}$ per unit AOD, is found to range from -0.39 to -2.75 $^{\circ}\text{C}$ per unit AOD. This aerosol cooling effect is observable for all four seasons for East Asia and India regions, as season mean AODs are higher than 0.3 for all four seasons for the two regions. For East Asia in particular, the aerosol cooling effect ranges from -1.5 to -2.5 $^{\circ}\text{C}$ per unit AOD for spring, summer and fall seasons and is -0.5 $^{\circ}\text{C}$ per unit AOD for the winter season. It is possible that the difference in aerosol cooling effect is introduced by different aerosol species from different seasons, as pollutant aerosols are likely dominant in the region during the winter season while dust aerosols dominate the spring season, which shows the highest mean AOD and the largest aerosol cooling effect in magnitude of -2.5 $^{\circ}\text{C}$ per unit AOD. Still, it is also possible that numerical models have different forecasting accuracy for different seasons. Although different aerosol types are expected for different seasons in the India region, similar aerosol cooling effect of -2.0 to -2.75 $^{\circ}\text{C}$ per unit AOD are found

for four seasons. Regions with mean AOD higher than 0.3 are also found for the Middle East in spring, summer and fall seasons and for Mid-south Africa for fall and winter seasons. Negative aerosol cooling effect on the order of -0.39 to -2.63 °C per unit AOD are found for those seasons, however, trends are statistically insignificant for the Mid-south Africa region for seasons with mean AOD values larger than 0.3.

For regions with seasonal mean AOD less than 0.3, however, the aerosol cooling effect is less observable and both negative and positive slopes between ΔT and AOD are found. It is not surprising, however, as with low aerosol loadings, aerosol cooling effect may be less significant in magnitude compared with inherited uncertainties in models.

Table 5. Similar to Table 4, but for using UKMO data.

Area	Season	Slope	95% confidence	Total data	Mean AOD	AOD value ratio (%)	
			interval			points	>0.5
East Asia	Spring	-0.86	[-0.94, -0.79]	10,955	0.61	47.14	18.36
	Summer	-0.85	[-1.02, -0.67]	3,174	0.46	32.42	10.11
	Fall	-1.75	[-1.86, -1.63]	8,376	0.31	18.74	3.88
	Winter	-1.30	[-1.40, -1.20]	13,327	0.33	20.29	3.78
India	Spring	-0.56	[-0.66, -0.45]	12,142	0.5	41.85	7.03
	Summer	-2.07	[-1.16, -0.91]	3,200	0.96	79.94	43.16
	Fall	-1.11	[-1.18, -1.03]	13,949	0.54	44.32	10.93
	Winter	-0.49	[-0.55, -0.42]	21,620	0.52	39.05	13.02
Europe	Spring	0.43	[0.43, 0.43]	26,775	0.14	2.25	0.09
	Summer	-0.43	[-0.69, 0.22]	53,758	0.19	3.69	0.23
	Fall	-0.32	[-0.59, 0.34]	36,303	0.13	1.86	0.22
	Winter	0.52	[0.52, 0.52]	15,133	0.09	0.46	0
US	Spring	0.79	[0.28, 1.14]	90,289	0.11	0.45	0
	Summer	-0.12	[-0.32, 0.16]	131,853	0.19	4.60	1.46
	Fall	-0.56	[-0.76, -0.15]	122,546	0.1	2.10	0.74
	Winter	0.39	[0.33, 0.95]	56,743	0.06	0	0
	Spring	-1.47	[-2.87, -0.08]	690	0.12	0	0

Area	Season	Slope	95% confidence interval	Total data points	Mean AOD	AOD value ratio (%)	
						>0.5	>1.0
North East Asia	Summer	0.24	[-0.09, 0.58]	1,777	0.24	13.67	4.84
	Fall	-0.83	[-1.55, -0.14]	1,731	0.1	1.91	0
	Winter	-7.41	[-26.55, 9.45]	133	0.11	0	0
Mid-south Africa	Spring	1.11	[-3.02, 4.82]	127	0.11	0	0
	Summer	0.53	[0.08, 0.97]	1,237	0.23	11.16	0
	Fall	0.92	[0.17, 1.64]	518	0.34	21.24	0
	Winter	0.27	[-0.95, 1.61]	106	0.53	25.84	1.87
Middle East	Spring	-0.17	[-0.39, 0.06]	4,394	0.43	29.59	4.46
	Summer	0.06	[-0.09, 0.21]	7,384	0.51	40.99	6.07
	Fall	-0.46	[-0.64, -0.27]	5,751	0.38	21.07	3.62
	Winter	-0.87	[-1.17, -0.57]	4625	0.24	15.21	0
South America	Spring	-1.59	[-2.96, -0.22]	841	0.15	0	0
	Summer	-1.72	[-2.39, -1.05]	2271	0.11	1.98	0
	Fall	-0.66	[-1.04, -0.28]	1405	0.28	13.02	2.56
	Winter	-1.38	[-2.74, -0.01]	410	0.22	3.77	0

Similar results are also found using UKMO data (Table 5) for the Indian and East Asia regions where mean AOD of higher than 0.3 are expected for all seasons. The aerosol cooling effect ranges from -0.85 to -1.75 °C per unit AOD for all seasons for East Asia. While for India, the aerosol cooling effect ranges from -0.49 to -0.56 °C per unit AOD for winter and spring season respectively and -1.11 °C per unit AOD for the fall season and -2.07 °C per unit AOD for the summer season. For the Mid-south Africa and Middle East regions, however, weakly negative and even positive aerosol cooling efficiencies are found, even for seasons with a mean AOD larger than 0.3. This is likely, although not conclusively known to be, due to the difference in model performance or due to insufficient data samples used in the analysis. Lastly, mixed negative and positive aerosol cooling efficiencies are

also found for other regions with less than 0.3 mean seasonal AOD values, which is similar to what we observed for using the NCEP data.

Overall, this study suggests that aerosol induced surface cooling effect should be taken into consideration in numerical weather prediction models for India and East Asia for all seasons, and for Middle East for spring, summer and fall seasons. For other regions, heavy aerosol plumes exist only during sporadically occurring events; thus, event-based methods may need to be developed to account for aerosol cooling effects over those regions.

4.4 Impacts of Cloud Contamination on Aerosol Cooling Effects

To study the impact of cloud coverage on aerosol induced surface cooling, as the reference to the clear sky condition (0 okta), two other observing conditions, partly cloudy (1-3 oktas), and mostly cloudy (4-6 oktas) are selected for three regions (East Asia, India, The Mid-East) that are previously identified as regions with significant aerosol surface cooling effect. No overcast conditions are selected as MODIS DT aerosol retrievals are not available over cloudy skies. The results are as shown in Table 6 to Table 9.

Table 6. Aerosol cooling efficiency ($^{\circ}\text{C}/\tau_{550\text{nm}}$) under three sky conditions for NCEP and UKMO models for spring for three selected regions. Also included are mean MODIS AOD, AEROENT Angstrom exponent (α) and 95% confident intervals for slopes (aerosol cooling efficiencies).

Area	Cloud cover (Oktas)	Slope/Total data points ($^{\circ}\text{C}/\tau_{550\text{nm}}$ /number of points)		Mean AOD ($\tau_{550\text{nm}}$)	95% confidence interval for slopes	
		NCEP	UKMO		NCEP	UKMO
East Asia	0	-2.50/11182	-0.86/10,955	0.61	[-2.61, -2.40]	[-0.94, -0.79]
	1-3	-2.53/17266	-1.04/17,078	0.51	[-2.62, -2.44]	[-1.11, -0.98]
	4-6	-1.99/11906	-1.02/11,777	0.61	[-2.07, -1.90]	[-1.08, -0.95]
India	0	-2.28/12553	-0.56/12,142	0.50	[-2.41, -2.15]	[-0.66, -0.45]
	1-3	-2.13/8254	-0.12/8,100	0.52	[-2.33, -1.94]	[-0.28, 0.05]
	4-6	-2.01/6049	-0.25/5,982	0.66	[-2.19, -1.82]	[-0.38, -0.11]

Area	Cloud cover (Oktas)	Slope/Total data points (°C/ τ_{550nm} /number of points)		Mean AOD (τ_{550nm})	95% confidence interval for slopes	
The	0	-0.39/4360	-0.17/4,394	0.43	[-0.67, -0.11]	[-0.39, 0.06]
Middle	1-3	-0.45/1955	-0.02/1,948	0.42	[-0.85, -0.06]	[-0.37, 0.32]
East	4-6	-1.37/983	-0.64/962	0.55	[-1.87, -0.87]	[-1.06, -0.23]

Table 7. Similar to Table 6, but for the summer season.

Area	Cloud cover (Oktas)	Slope/Total data points (°C/ τ_{550nm} /number of points)		Mean AOD (τ_{550nm})	95% confidence interval for slopes	
		NCEP	UKMO		NCEP	UKMO
East Asia	0	-1.67/2796	-0.85/3,174	0.46	[-1.91, -1.42]	[-1.02, -0.67]
	1-3	-1.69/9611	-1.12/10,635	0.33	[-1.85, -1.53]	[-1.23, -1.01]
	4-6	-1.28/9619	-0.90/10,608	0.40	[-1.28, -1.28]	[-0.90, -0.90]
India	0	-2.50/3058	-1.03/3,200	0.96	[-2.70, -2.30]	[-1.16, -0.91]
	1-3	-4.14/3008	-2.07/3,302	0.71	[-4.35, -3.93]	[-2.22, -1.93]
	4-6	-3.07/4089	-1.41/4,544	0.74	[-3.23, -2.91]	[-1.51, -1.31]
The Middle East	0	-0.83/6692	0.06/7,384	0.51	[-1.02, -0.64]	[-0.09, 0.21]
	1-3	-1.13/1420	-0.01/1,582	0.59	[-1.61, -0.66]	[-0.39, 0.36]
	4-6	0.14/449	-0.19/495	0.69	[-0.84, 1.12]	[-0.91, 0.53]

Table 8. Similar to Table 6, but for the fall season.

Area	Cloud cover (Oktas)	Slope/Total data points (°C/ τ_{550nm} /number of points)		Mean AOD (τ_{550nm})	95% confidence interval for slopes	
		NCEP	UKMO		NCEP	UKMO
East Asia	0	-2.23/8209	-1.75/8,376	0.31	[-2.39, -2.08]	[-1.86, -1.63]
	4-6	-0.96/10245	-1.03/10,541	0.30	[-0.96, -0.96]	[-1.03, -1.03]
India	0	-2.75/13494	-1.11/13,949	0.54	[-2.87, -2.64]	[-1.18, -1.03]
	1-3	-2.48/6822	-1.81/7,041	0.38	[-2.67, -2.30]	[-1.96, -1.66]
	4-6	-1.38/5198	-0.91/5,343	0.45	[-1.55, -1.21]	[-1.04, -0.78]
The Middle East	0	-0.56/5598	-0.46/5,751	0.38	[-0.80, -0.33]	[-0.64, -0.27]
	1-3	0.31/1937	0.46/2,016	0.38	[-0.15, 0.78]	[0.11, 0.80]
	4-6	-1.10/592	-0.81/605	0.47	[-1.80, -0.41]	[-1.31, -0.31]

Table 9. Similar to Table 6, but for the winter season.

Area	Cloud cover (Oktas)	Slope/Total data points ($^{\circ}\text{C}/\tau_{550\text{nm}}$ /number of points)		Mean AOD ($\tau_{550\text{nm}}$)	95% confidence interval for slopes	
		NCEP	UKMO		NCEP	UKMO
East Asia	0	-0.50/12698	-1.30/13,327	0.33	[-0.62, -0.38]	[-1.40, -1.20]
	4-6	-2.10/8351	-1.49/8,878	0.33	[-2.25, -1.95]	[-1.61, -1.38]
India	0	-2.04/20323	-0.49/21,620	0.52	[-2.12, -1.96]	[-0.55, -0.42]
	1-3	-1.69/7924	-0.80/8,393	0.38	[-1.87, -1.51]	[-0.94, -0.65]
	4-6	-1.87/4228	-0.50/4,515	0.58	[-2.05, -1.69]	[-0.63, -0.38]

For the East Asia and India regions, regardless of cloud conditions, an overall aerosol cooling effect is observed. The aerosol cooling effect ranges from -2.01 to -2.28 $^{\circ}\text{C}/\tau_{550\text{nm}}$ from Indian during the spring season, using UKMO data, to -2.50 to -4.14 $^{\circ}\text{C}/\tau_{550\text{nm}}$ for the Indian region for the summer season using NCEP data. No clear relationship, however, is found between cloud fraction and aerosol cooling effect.

Positive aerosol cooling effects are also observed for the Middle East region over summer and fall season, which could be caused by data sample size. For example, a total of 495 validate data point is available for using NCEP data during the summer season under mostly cloudy condition, however, a total of 7384 data points is used for the similar situation for the cloud free condition.

4.5 Impact of Aerosol Type on Aerosol Surface Cooling

For different regions under different seasons, distinct types of aerosol particles may exist. For example, over the east coast of China, dust aerosols are reported during spring (Zhang et al, 2017) while pollutant aerosols are reported during winter (Zhang et al., 2017). Therefore, it is interesting to study the impact of the individual aerosol type on aerosol

induced surface cooling. To achieve this goal, for each region and season averaged aerosol Angstrom exponent values are used as a proxy for aerosol type. Here aerosol events can be divided into two dominated aerosol types based on the value of α (Eck et al., 1999): fine model aerosols such as biomass burning / Urban pollution ($\alpha \geq 1$), and coarse model aerosols such as desert dust ($\alpha \ll 1$). Also included in the Table 10 are the fine mode aerosol fraction values. Similar to Angstrom Exponent, the fine mode fraction can be used to indicate particle size, with near zero values indicate coarse model aerosol domination and values near 1 refer fine mode aerosol domination.

Table 10. Seasonal variations of aerosol cooling efficiency ($^{\circ}\text{C}/\tau_{550\text{nm}}$) for the East Asia, India and the Middle East regions under cloud-free condition using NCEP and UKMO data.

Area	Season	Slope($^{\circ}\text{C}/\tau_{550\text{nm}}$) NCEP/UKMO	α -value	Fine model fraction
East Asia	Spring	-2.50/-0.86	1.37	0.88
	Summer	-1.67/-0.85	1.25	0.77
	Fall	-2.23/-1.75	1.24	0.82
	Winter	-0.50/-1.30	1.28	0.86
India	Spring	-2.28/-0.56	0.95	0.51
	Summer	-2.50/-1.03	0.93	0.47
	Fall	-2.75/-1.11	1.02	0.59
	Winter	-2.04/-0.49	1.14	0.74
The Middle East	Spring	-0.39/-0.17	0.31	0.12
	Summer	-0.83/0.06	0.50	0.08
	Fall	-0.56/-0.46	0.78	0.21
	Winter		N/A	

For the East Asia region, as indicated from Table 10, seasonally averaged AERONET α values of above 1 are found for all four seasons. In comparison, seasonal mean α values are 1.14 and 0.93 for the winter and the summer season respectively for the India region. It is not surprising as pollutant aerosols are expected during winter months

over the India region while dust and sea salt aerosols, which are both coarse model aerosols, are expected during the summertime, due to the summer monsoon of the region. Correspondingly, aerosol cooling efficiencies of -2.04 and -0.49 °C/ $\tau_{550\text{nm}}$ are found for the winter season using NCEP and UKMO data respectively. Similarly, for the summer season aerosol cooling efficiencies of -2.50 and -1.03 °C/ $\tau_{550\text{nm}}$ are found using NCEP and UKMO data respectively. This seems suggesting that a larger aerosol cooling efficiency (in absolute value) can be expected for the presence of coarse mode aerosols. Yet, much lower aerosol cooling efficiency (in absolute value) values are found over the Middle East region that have low mean α values ranging from 0.31 to 0.78. Therefore, we may suspect that larger aerosol cooling efficiency (in absolute value) values can be expected for fine model aerosols, yet this conclusion is not supported by analyses within a region such as the India region.

4.6 Aerosol Cooling Induced Bias as A Function of Forecast Hours

While previous sections studied the impacts of aerosol on NCEP and UKMO analyses, which include data assimilation in the process. UKMO and NCEP forecasts up to 48 hours are also available for this study. Therefore, the impacts of aerosol particles on forecasted temperatures from both NCEP and UKMO model are studied as a function of forecasting hour as shown in Table 11 and Table 12.

Table 11. The variations of seasonal-based aerosol cooling efficiency ($^{\circ}\text{C}/\text{AOD}$) for 0h, 24h and 48h forecasts for the East Asia and India regions using NCEP model data. Also included are forecasting periods, 95% confident intervals of the computed slopes as well as mean and median of ΔT values.

Aera	Season	Forecast period (h)	Slope($^{\circ}\text{C}/\tau_{550\text{nm}}$)	95 % confidence interval	Mean/median of ΔT bias ($^{\circ}\text{C}$)
East Asia	Spring	00	-2.50	[-2.61, -2.40]	0.32/0.28
		24	-2.91	[-3.03, -2.79]	0.05/-0.02
		48	-3.03	[-3.16, -2.91]	0.10/0.04
	Summer	00	-1.67	[-1.91, -1.42]	1.09/1.01
		24	-2.15	[-2.43, -1.87]	0.65/0.67
		48	-2.29	[-2.59, -2.00]	0.55/0.50
	Fall	00	-2.23	[-2.39, -2.08]	1.29/1.07
		24	-2.70	[-2.86, -2.54]	1.48/1.29
		48	-2.75	[-2.93, -2.58]	1.55/1.41
	Winter	00	-0.50	[-0.62, -0.38]	0.35/0.34
		24	-0.71	[-0.85, -0.57]	0.62/0.59
		48	-0.36	[-0.51, -0.21]	0.85/0.85
India	Spring	00	-2.28	[-2.41, -2.15]	-1.75/-1.80
		24	-2.61	[-2.75, -2.46]	-1.72/-1.71
		48	-2.46	[-2.61, -2.32]	-1.84/-1.84
	Summer	00	-2.50	[-2.70, -2.30]	-2.88/-3.36
		24	-2.06	[-2.27, -1.84]	-2.79/-3.13
		48	-1.93	[-2.15, -1.71]	-2.86/-3.08
	Fall	00	-2.75	[-2.87, -2.64]	-1.35/-1.19
		24	-2.63	[-2.74, -2.52]	-0.89/-0.81
		48	-2.74	[-2.86, -2.62]	-0.97/-0.91
	Winter	00	-2.04	[-2.12, -1.96]	-1.51/-1.44
		24	-2.11	[-2.18, -2.03]	-1.28/-1.30
		48	-2.09	[-2.17, -2.01]	-1.37/-1.39

Table 12. Similar to Table 11, but for using UKMO model data.

Aera	Season	Forecast period (h)	Slope($^{\circ}\text{C}/\tau_{550\text{nm}}$)	95 % confidence interval	Mean/median of ΔT bias ($^{\circ}\text{C}$)
	Spring	00	-0.86	[-0.94, -0.79]	1.27/1.15
		24	-1.58	[-1.68, -1.49]	1.39/1.28
		48	-1.79	[-1.89, -1.69]	1.45/1.31

Aera	Season	Forecast period (h)	Slope($^{\circ}\text{C}/\tau 550\text{nm}$)	95 % confidence interval	Mean/median of ΔT bias ($^{\circ}\text{C}$)
East Asia	Summer	00	-0.85	[-1.02, -0.67]	1.18/1.04
		24	-1.32	[-1.52, -1.11]	1.24/1.15
		48	-1.27	[-1.51, -1.03]	1.27/1.19
	Fall	00	-1.75	[-1.86, -1.63]	1.60/1.42
		24	-1.86	[-1.99, -1.73]	2.25/2.10
		48	-1.56	[-1.72, -1.41]	2.52/2.39
	Winter	00	-1.30	[-1.40, -1.20]	1.45/1.35
		24	-1.41	[-1.53, -1.30]	1.96/1.89
		48	-1.18	[-1.31, -1.04]	2.30/2.25
India	Spring	00	-0.56	[-0.66, -0.45]	-0.44/-0.55
		24	-1.27	[-1.39, -1.15]	-0.33/-0.40
		48	-1.40	[-1.53, -1.27]	-0.43/-0.49
	Summer	00	-1.03	[-1.16, -0.91]	-0.55/-0.76
		24	-1.44	[-1.61, -1.28]	-0.89/-1.08
		48	-1.59	[-1.77, -1.41]	-1.29/-1.49
	Fall	00	-1.11	[-1.18, -1.03]	-0.01/0.03
		24	-1.65	[-1.74, -1.56]	-0.04/0.04
		48	-1.79	[-1.89, -1.69]	-0.16/-0.08
	Winter	00	-0.49	[-0.55, -0.42]	0.10/0.13
		24	-0.87	[-0.94, -0.81]	0.18/0.17
		48	-1.15	[-1.22, -1.08]	0.06/0.05

As shown in Table 11, a decreasing trend of cooling efficiency is found over four seasons for 0 to 24h forecast periods and spring, summer and fall seasons for 24 to 48h forecast periods over East Asia using NCEP model data. Yet the decreasing trend is less observable for the India region.

A similar analysis is also processed by using data from UKMO model as shown in Table 12. A relatively decreasing trend of cooling efficiency is found for all four seasons over the India region from 0 to 48h forecast periods, and four seasons over East Asia region for 0 to 24h forecast periods and spring for 24 to 48h forecast periods. Note relatively

increasing trends also exist for certain forecast periods for the results from both NCEP and UKMO models.

Although there is an overall decreasing trend in aerosol cooling efficiency as a function of forecasting hour, there are cases where aerosol cooling trends are independent of forecasting hour. We suspect that this aerosol cooling efficiency trend is likely also linked to the forecasting accuracies of different models at different forecasting hours.

4.7 Issues and Discussions

Note that the results of the study may be affected by uncertainties in data from few sources as identified below:

1. Over partially cloudy or mostly cloudy regions, aerosol retrievals could still be available. However, as suggested from Zhang et al. (2005), a bias may exist in those AOD retrievals due to misclassification of cloud signals as aerosol signals. Also, very optically thin cirrus clouds, which are difficult to detect using MODIS observations alone, may introduce a high bias in AOD over optically thin cloud contaminated regions.

2. The effect of cloud cover on aerosol induced surface cooling effect was studied; yet, different clouds, with different cloud type (e.g. ice versus water) and different optical properties (such as optical depth, effective radius), will have different scattering properties. Therefore, over partially cloudy or mostly cloudy skies, aerosol induced surface cooling effect should also be a function of cloud optical and physical properties. However, no effort was applied in this study to quantify cloud optical and physical properties as that would be a whole study of its own on both a regional and global scale.

3. Aerosol type is quantified based on AERONET reported Angstrom Exponent / fine model values. Yet, aerosol Angstrom Exponent / fine mode fraction can only be used to quantify aerosol particle size and it is rather plausible to link aerosol Angstrom Exponent /fine mode fraction to aerosol type. Also, AERONET data are only available over limited ground based AERONET sites. Both of which will unavoidably introduce an uncertainty in this study.

4. Since the AERONET could only provide ground aerosol data from few locations on a global scale, for a larger study region, the value of α might not be representative due to the relative sparse of AERONET stations over a large study area.

CHAPTER5

CONCLUSIONS

Using collocated observational data from ISD, MODIS, AERONET, as well as modeling data from NCEP and UKMO models, the aerosol induced biases on NCEP and UKMO forecasted 2-m temperatures are studied (aerosol cooling effect). Major findings are as follows:

1. The aerosol induced surface cooling effect is only clearly observable over regions / seasons with high mean AOD value ($AOD \geq 0.3$), such as all seasons for East Asia and India, and spring, summer and fall seasons for the Middle East region. Those are the regions and seasons that the impacts of aerosols on weather forecasts should be fully considered in future studies.

2. For regions with lower seasonal mean AODs, aerosol surface cooling effects are less observable and are often statistically insignificant. This suggests that the impacts of aerosols on weather can be considered on event-based scenarios and methods needed to be developed to account for the impacts of aerosol particles on numerical weather forecasts only over days with heavy aerosol events such as biomass burning events or dust storms. For example, the US region has annually low mean AOD value, however, a former study (Zhang et al., 2016) indicated that forecasted surface temperature could be impacted by biomass burning events in a short period.

3. The aerosol cooling effect was also studied as a function of cloud coverage. However, no clear impact is found. The real reason is not known. This may be due to uncertainties in both models and observations under cloudy skies.

4. Through the use of AERONET data, aerosol cooling effect is studied as a function of AERONET Angstrom Exponent (α) values. A higher aerosol cooling efficiency (in absolute value) is found for regions with α larger than 1, which is indicative of fine mode aerosols such as smoke aerosols. Still, this conclusion is less robust as within the India and East Asia regions, however, higher aerosol cooling efficiencies (in absolute value) are observed for dust dominated seasons.

5. A plausible relationship is also found between aerosol cooling efficiency and forecasting hour. For most studied cases over East Asia and India, a decrease in aerosol cooling efficiency is found as forecast hour increases. However, there are also cases that aerosol cooling efficiency is independent of forecasting hour, indicating other factors such as model uncertainties could also affect the analysis.

Clearly, aerosol particles could affect regional weather and regional weather forecasts. This study further evaluated the impacts and demonstrated the need to consider aerosol cooling effects in numerical weather forecasts. As the natural extension from the study, new methods can and should be explored to incorporate aerosol particles, either through in-line or off-line modes, for accounting this aerosol cooling effect for improved weather forecasts over regions as highlighted in the study.

APPENDIX

Appendix A

Table 13. Total number of missing data from NCEP model (Data are not available from the TIGGE site), ‘-’ represents no missing data for a given forecasting/analysis period.

Date	Forecast Period											
	0000	0024	0048	0600	0624	0648	1200	1224	1248	1800	1824	1848
2014.12	-	-	-	1	1	1	1	1	1	-	-	-
2015.1	1	1	1	4	4	4	3	3	3	1	1	1
2015.2	2	2	2	-	-	-	-	-	-	1	1	1
2015.5	-	-	-	1	1	1	-	-	-	1	1	1
2015.6	-	-	-	-	-	-	-	-	-	3	3	3
2015.7	-	-	-	-	-	-	-	-	-	3	3	3
2015.8	-	-	-	1	1	1	1	1	1	1	1	1
2015.12	11	11	11	12	12	12	10	10	10	-	-	-
2016.1	-	-	-	-	-	-	-	-	-	1	1	1
2016.2	-	-	-	-	-	-	-	-	-	1	1	1
2016.5	-	-	-	-	-	-	1	1	1	-	-	-
2016.6	6	6	6	8	8	8	9	9	9	7	7	7
2016.7	7	7	7	5	5	5	5	5	5	5	5	5
2016.8	9	9	9	12	12	12	10	10	10	10	10	10
2016.9	1	1	1	2	2	2	2	2	2	3	3	3
2016.10	2	2	2	2	2	2	4	4	4	2	2	2
2016.11	2	2	2	4	4	4	4	4	4	2	2	2
2016.12	1	1	1	2	2	2	1	1	1	1	1	1
2017.3	-	-	-	3	3	3	2	2	2	-	-	-
2017.10	1	1	1	-	-	-	-	-	-	1	1	1
2017.11	1	1	1	-	-	-	-	-	-	-	-	-
2017.12	2	2	2	-	-	-	1	1	1	-	-	-
Total	46	46	46	57	57	57	54	54	54	43	43	43

Table 14. Similar to Table 13, but for UKMO model.

Date	Forecast Period											
	0000	0024	0048	0600	0624	0648	1200	1224	1248	1800	1824	1848
2015.1	-	-	-	1	1	1	1	1	1	-	-	-
2016.3	1	1	1	1	1	1	1	1	1	-	-	-
2017.3	6	6	6	6	6	6	6	6	6	-	-	-
Total	7	7	7	8	8	8	8	8	8	0	0	0

Appendix B

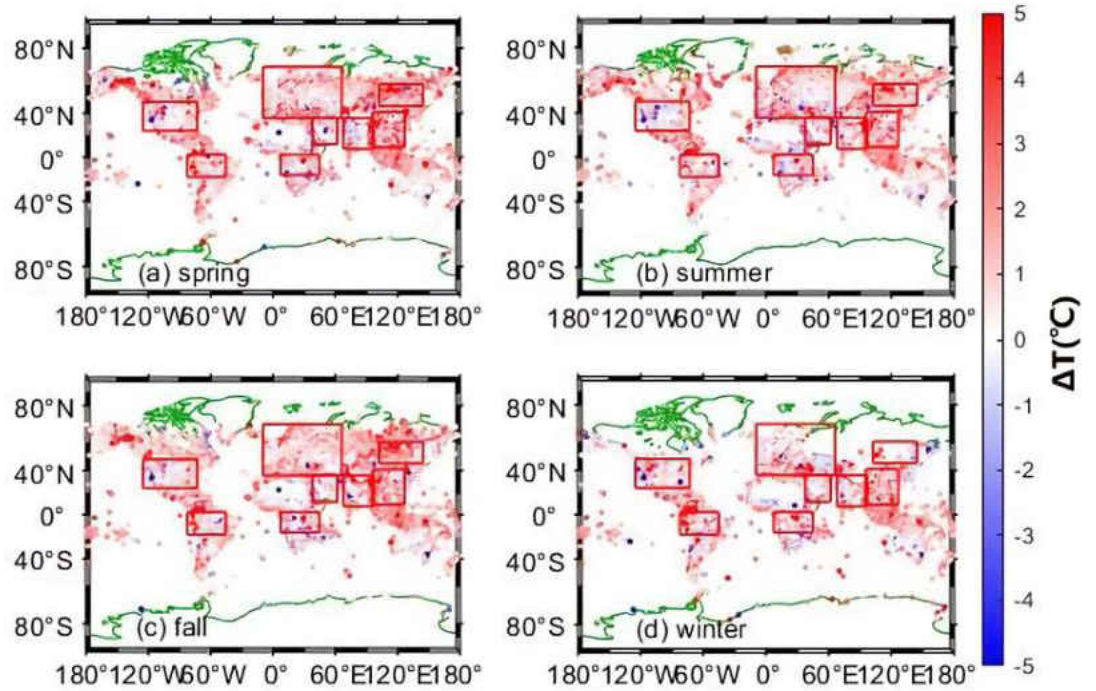


Figure 8. 3-year averaged seasonal mean 2-m temperature biases (observation temperature – forecasted temperature, in °C) for UKMO model over ISD stations for Northern Hemisphere (a) spring, (b) summer, (c) fall and (d) winter. Red boxes highlight focused study regions.

Appendix C

Table 15. Acronyms and Definitions.

Acronym	Definition
AERONET	Aerosol Robotic NET Work
AOD	Aerosol Optical Depth
CCN	Cloud Condensation Nuclei
DT	Dark Target
GFS	Global Forecast System
GSI	Grid Point Statistical Interpolation
ISD	Integrated Surface Database
LUT	Look Up Table
MODIS	Moderate Resolution Imaging Spectroradiometer
NCEP	National Centers for Environmental Prediction
TIGGE	THORPEX Interactive Grand Global Ensemble
TOA	Top of Atmosphere
UKMO	United Kingdom Met Office

REFERENCES

- Ångström, A. (1929). On the Atmospheric Transmission of Sun Radiation and on Dust in the Air. *Geografiska Annaler*, 11, 156-166. doi:10.2307/519399
- Charlson, R.J., S.E. Schwartz, J.M. Hales, R.D. Cess, J.A. Coakley, Jr., J.E. Hansen, and D.J. Hoffman, 1992: Climate forcing by anthropogenic aerosols. *Science*, 255, 423-430, doi:10.1126/science.255.5043.423.
- Eck, T. F., Holben, B. N., Reid, J. S., Dubovic, O., Smirnov, A., O'Neill, N. T., Slutsker, I., and Kinne, S.: The wavelength dependence of the optical depth of biomass burning, urban and desert dust aerosols, *J. Geophys. Res.*, 104, 31333–31350, 1999.
- Giles DM, Sinyuk A, Sorokin MG, et al. Advancements in the Aerosol Robotic Network (AERONET) Version 3 database – automated near-real-time quality control algorithm with improved cloud screening for Sun photometer aerosol optical depth (AOD) measurements. *Atmospheric Measurement Techniques*. 2019;12(1):169-209. doi:10.5194/amt-12-169-2019.
- Gilbert, Richard O. *Statistical Methods for Environmental Pollution Monitoring*. United States: N. p., 1987. Web.
- Gupta, P., Levy, R. C., Mattoo, S., Remer, L. A., and Munchak, L. A.: A surface reflectance scheme for retrieving aerosol optical depth over urban surfaces in MODIS Dark Target retrieval algorithm, *Atmos. Meas. Tech.*, 9, 3293–3308, <https://doi.org/10.5194/amt-9-3293-2016>, 2016.
- Holben, B. N., Eck, T. F., Slutsker, I., Tanré, D., Buis, J. P., Setzer, A., ... Smirnov, A. (1998). AERONET - A federated instrument network and data archive for aerosol

- characterization. *Remote Sensing of Environment*, 66(1), 1-16.
[https://doi.org/10.1016/S0034-4257\(98\)00031-5](https://doi.org/10.1016/S0034-4257(98)00031-5)
- J.A. Coakley Jr., R.D. Cess, F.B. Yurevich The effect of tropospheric aerosols on the earth's radiation budget: a parameterisation for climate models *Journal of Atmospheric Science*, 40 (1983), pp. 116-138
- Jr, Coakley, & Cess, Robert & Yurevich, Franz. (1982). The Effect of Tropospheric Aerosols on the Earth's Radiation Budget: A Parameterization for Climate Models. *Journal of Atmospheric Sciences*. 40. 116-138. 10.1175/1520-0469(1983)040<0116:TEOTAO>2.0.CO;2.
- Kendall, M.G., 1975. Rank Correlation Methods. Griffin, London, UK
- Kleist, D. T., D. F. Parrish, J. C. Derber, R. Treadon, W.-S. Wu, and S. Lord, 2009: Introduction of the GSI into the NCEP Global Data Assimilation System. *Wea. Forecasting*, 24, 1691–1705
- Lee, Jaehwa & Kim, Jhoon & Lee, Hee & Takemura, Toshihiko. (2007). Classification of aerosol type from MODIS and OMI over East Asia. *J. Kor. Meteor. Soc.*. 43. 343-357.
- Levy, R. C., Remer, L. A., Kleidman, R. G., Mattoo, S., Ichoku, C., Kahn, R., and Eck, T. F.: Global evaluation of the Collection 5 MODIS dark-target aerosol products over land, *Atmos. Chem. Phys.*, 10, 10399–10420, doi:10.5194/acp-10-10399-2010, 2010
- Lott, N., R. Baldwin, and P. Jones, 2001: The FCC integrated surface hourly database. NCDC Tech. Rep. 2001–01, Asheville, NC, 42 pp.
- Mann, H.B., 1945. Nonparametric tests against trend. *Econometrica* 13, 245–259

- O'Neill, N. T., T. F., Eck, A. Smirnov, B. N. Holben, S. Thulasiraman, Spectral discrimination of coarse and fine mode optical depth, *J. Geophys. Res.*, Vol. 108, No. D17, 4559-4573, 10.1029/2002JD002975, 2003.
- Painemal, D. and Zuidema, P.: The first aerosol indirect effect quantified through airborne remote sensing during VOCALS-REx, *Atmos. Chem. Phys.*, 13, 917–931, <https://doi.org/10.5194/acp-13-917-2013>, 2013.
- Rousseeuw, Peter J.; Leroy, Annick M. (2003), *Robust Regression and Outlier Detection*, Wiley Series in Probability and Mathematical Statistics, 516, Wiley, p. 67, ISBN 978-0-471-48855-2.
- Sen, Pranab Kumar (1968), "Estimates of the regression coefficient based on Kendall's tau", *Journal of the American*
- Theil, H. (1950), "A rank-invariant method of linear and polynomial regression analysis. I, II, III", *Nederl. Akad. Wetensch., Proc.*, 53: 386–392, 521–525, 1397–1412, MR 0036489
- Wang, Y., Wang, M., Zhang, R., Ghan, S. J., Lin, Y., Hu, J., Pan, B., Levy, M., Jiang, J. H., & Molina, M. J. (2014). Assessing the effects of anthropogenic aerosols on Pacific storm track using a multiscale global climate model. *Proceedings of the National Academy of Sciences of the United States of America*, 111(19), 6894–6899. <https://doi.org/10.1073/pnas.1403364111>
- Zhang, J., J. S. Reid, M. Christensen, and A. Benedetti, 2016: An evaluation of the impact of aerosol particles on weather forecasts from a biomass burning aerosol event over the Midwestern United States: Observational-based analysis of surface

temperature. *Atmos. Chem. Phys.*, 16, 6475–6494, <https://doi.org/10.5194/acp-16-6475-2016>.

Zhang, Jiandong & Reid, Jeffrey & Alfaro, Ricardo & Xian, Peng. (2017). Has China been exporting less particulate air pollution over the past decade?: China air pollution. *Geophysical Research Letters*. 10.1002/2017GL072617.

Zhang, Jiandong & Reid, Jeffrey & Holben, Brent. (2005). An analysis of potential cloud artifacts in MODIS over ocean aerosol optical thickness products. *GEOPHYSICAL RESEARCH LETTERS*. 32. 10.1029/2005GL023254.